International Journal of Microwave and Wireless Technologies

cambridge.org/mrf

Modifications of active phased antenna arrays near-field diagnosis method based on compressive sensing

Grigory Kuznetsov[1], Vladimir Temchenko[2], Maxim Miloserdov[1] and Dmitry Voskresenskiy[2]

[1]Research Institute of Precision Instruments, Moscow, Russia and [2]Department of Radioelectronics, Moscow Aviation Institute, Moscow, Russia

Research Paper

Cite this article: Kuznetsov G, Temchenko V, Miloserdov M, Voskresenskiy D (2019). Modifications of active phased antenna arrays near-field diagnosis method based on compressive sensing. *International Journal of Microwave and Wireless Technologies* **11**, 568–576. https://doi.org/10.1017/S1759078719000989

Received: 14 October 2018
Revised: 17 June 2019
Accepted: 22 June 2019
First published online: 18 July 2019

Key words:
Antenna array; diagnostics; compressive sensing; inverse problem; thermal instability

Author for correspondence:
Grigory Kuznetsov, E-mail: grigory.kuznetsov@niitp.ru

Abstract

This paper presents two modifications of compressive sensing (CS)-based approach applied to the near-field diagnosis of active phased arrays. CS-based antenna array diagnosis allows a significant reduction of measurement time, which is crucial for the characterization of electrically large active antenna arrays, e.g. used in synthetic aperture radar. However, practical implementation of this method is limited by two factors: first, it is sensitive to thermal instabilities of the array under test, and second, excitation reconstruction accuracy strongly depends on the accuracy of the elements of the measurement matrix. First proposed modification allows taking into account of thermal instability of the array by using an iterative ℓ_1-minimization procedure. The second modification increases the accuracy of reconstruction using several simple additional measurements.

Introduction

Development, calibration, and testing of active phased antenna arrays require solving a large number of problems, including the problem of diagnosis of the array under test (AUT). Many factors determine the selection of the diagnosis method: structure and operating mode of AUT during the testing, diagnosis duration (including duration of measurement and computation), and cost of its implementation. The results of the diagnosis problem solution allow estimating the technical condition of the active array and determining how its characteristics differ from the required ones. These differences may be caused by failures of single or groups of transmit-and-receive modules (TRMs), including failures of phase shifters, switches, and amplifiers [1,2].

Especially strict performance requirements are imposed on space-borne systems, particularly synthetic aperture radars [2,3]. Ground testing of active arrays includes measuring not only radiation characteristics (far-field pattern, sidelobe level, equivalent isotropic radiated power, cross-polarization level, mutual coupling between elements) but also impedance matching, power loss, and power consumption.

Many radiation characteristics of electrically large active arrays can only be measured in an anechoic chamber using near-field techniques, because the far-field zone distance may be prohibitively large. After the initial calibration of the phase shifters and attenuators of the array, a testing in normal operating mode, i.e. with all TRMs turned on, is required.

On this step, a testing of the antenna in a wide temperature range (tens and hundreds °C) should be performed [4,5], since the characteristics of TRMs significantly depend on temperature. The measurement duration of active arrays compared to passive antennas is limited by three factors. First, the service life of TRMs is limited. Second, the TRMs warm up during the operation, and change their characteristics. Third, the duration of the normal operating mode of the whole system is also limited.

Conventional methods of phased antenna array diagnosis include measurement of the full set of field data in the near- or far-field zone [6,7]. These methods, including methods based on the solution of integral equations using the method of moments, do not utilize *a priori* information about a reference, non-defect array. It leads to a large dimensionality of the problem, and the resulting computational problem is ill-posed [8]. For an array of N elements, the number of measurements M must be equal to or larger than N, and measurement duration may become prohibitively high, especially for electrically large arrays.

Along with conventional methods, new methods based on a "compressive sensing" (CS) approach are developed [9,10]. These methods can also be applied to similar related problems, such as "inverse scattering" [11,12]. Provided that the number of defects is low, these methods allow a significant reduction of the number of measurements by using *a priori* information about the field radiated by the reference (non-defect) array. While the idea behind CS-based diagnosis is very simple, there are still a number of unanswered questions:

© Cambridge University Press and the European Microwave Association 2019

CAMBRIDGE UNIVERSITY PRESS

1. How many measurements should be conducted to locate K defect elements among N elements with required probability?
2. How measurement points' locations should be chosen?
3. What can be done if the temperature of the AUT differs from the temperature of the reference array?
4. Is it possible to reconstruct the excitation if the elements of the measurement matrix are not known exactly, e.g. when far-field patterns of radiating elements or measurement probe are not known, or if the reflections are present?

The first two questions received attention in the literature, e.g. good estimates of the required minimum number of measurements exist for a case of far-field measurement. In [13], the second problem was solved but also for the far-field case; for the near-field case, only a numerical example is shown in [14].

However, the remaining questions were not investigated in detail. Existing research shows that (a) the change in excitation due to temperature drift lowers the probability of failure detection and increases the rate of false positives [5,15]; (b) errors in the measurement matrix also lead to low accuracy of excitation reconstruction [16].

This paper presents and discusses in detail two modifications of CS-based diagnosis method that are focused on improving the quality (i.e. raising the probability of detection and lowering the probability of false detection (PFD)) and accuracy of diagnosis.

The first approach is aimed at a compensation of possible temperature drift of the array's characteristics assuming that the amplitudes and phases of all elements changed by the same amount. An iterative procedure is carried out to determine the desired change in excitation and solve the diagnosis problem. The second modification consists of two steps focused on the improvement of reconstruction accuracy. On the first step, CS-based diagnosis is used to locate potentially defect elements. On the second step, a series of additional measurements is carried out when only the phase of a potentially defect element changes, but the position of the probe remains fixed. This approach increases the accuracy of reconstruction without increasing the measurement duration, since most of the time required for the measurement is taken by the probe moving, and not by the registration of measured field.

Compressive sensing approach to array diagnosis

Formulation of problem

Active phased antenna array diagnosis problem is carried out on the basis of the inverse problem solution and can be reduced to the finding of array elements' amplitudes and phases. The geometry of the problem is shown in Fig. 1. Radius vector $\mathbf{r}_n$ specifies the position of n-th ($n = 1,2, \ldots, N$) radiating element located in the aperture plane S_A, $\mathbf{r}_m$ is the position of m-th ($m = 1,2,\ldots, M$) measurement point in the measurement surface S_M. The field of each element is modeled by a set of elementary electric and magnetic dipoles, which are located at $\mathbf{r}^e_{kn}$ and $\mathbf{r}^m_{kn}$, $k = 1,2, \ldots, K$. Current distribution of the dipoles is given as:

$$\begin{aligned}\mathbf{j}^e_T(\mathbf{r}, \omega) &= p^e_{kn}\delta(\mathbf{r} - \mathbf{r}^e_{kn})\mathbf{p}^e_{0k}\\ \mathbf{j}^m_T(\mathbf{r}, \omega) &= p^m_{kn}\delta(\mathbf{r} - \mathbf{r}^m_{kn})\mathbf{p}^m_{0k},\end{aligned} \tag{1}$$

where $p^e_{kn}\mathbf{p}^e_{0k}$ and $p^m_{kn}\mathbf{p}^m_{0k}$ are the vector dipole moments, and $\mathbf{p}^e_{0k}$ and $\mathbf{p}^m_{0k}$ are the unit vectors that define the orientation of k-th dipole.

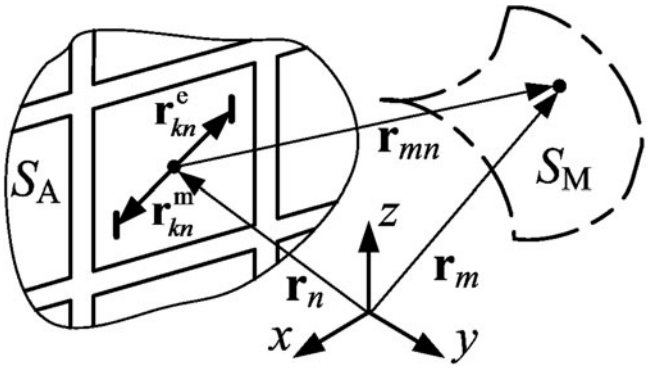


Fig. 1. Geometry of the problem.

The field of the n-th element at the m-th measurement point can be found as shown in [17]:

$$\mathbf{E}_{Dn}(\mathbf{r}_{mn}, \omega) = \mathbf{E}^e_{Dn}(\mathbf{r}_{mn}, \omega) + \mathbf{E}^m_{Dn}(\mathbf{r}_{mn}, \omega), \tag{2}$$

where

$$\begin{aligned}\mathbf{E}^e_{Dn}(\mathbf{r}_{mn}) &= \frac{ik_0 Z_0 \exp(-ik_0 r_{mn})}{4\pi r_{mn}}\\ &\quad\times\left[\sum_{k=1}^{N} p^e_{kn}\exp\left(i\,k_0\,\mathbf{r}^e_{kn}\mathbf{r}_{n0}\right)\left[\left(\mathbf{p}^e_{0k}\mathbf{r}_{n0}\right)\mathbf{r}_{n0} - \mathbf{p}^e_{0k}\right]\right]\\ &= \tilde{\mathbf{E}}^e_{Dn}(\mathbf{r}_{mn})\frac{\exp(-ik_0 r_{mn})}{r_{mn}}\end{aligned} \tag{3}$$

and

$$\begin{aligned}\mathbf{E}^m_{Dn}(\mathbf{r}_{mn}) &= -\frac{ik_0\exp(-ik_0\,r_{mn})}{4\pi r_{mn}}\times\left[\sum_{k=1}^{K} p^m_k\exp\left(ik_0\,\mathbf{r}^m_k\mathbf{r}_{n0}\right)\left[\mathbf{p}^m_{0k}\times\mathbf{r}_{n0}\right]\right]\\ &= \tilde{\mathbf{E}}^m_{Dn}(\mathbf{r}_{mn})\frac{\exp(-ik_0 r_{mn})}{r_{mn}},\end{aligned} \tag{4}$$

where k_0 is the wave number, $r_{mn} = |\mathbf{r}_m - \mathbf{r}_n|$ - distance from the element to the measurement point,$\mathbf{r}_{n0} = \mathbf{r}_{mn}/r_{mn}$, and it is taken into account that $r_{mn} \gg |\mathbf{r}^e_{kn}|$ and $r_{mn} \gg |\mathbf{r}^m_{kn}|$ (see Fig. 1). Assuming that the dipole moments in (3) and (4) are normalized, the radiated field (2) of the n-th element excited by the current with complex amplitude x_n can be found as

$$\begin{aligned}\mathbf{E}_{Dn}(\mathbf{r}_{mn}) &= x_n\left(\tilde{\mathbf{E}}^e_{Dn}(\mathbf{r}_{mn}) + \tilde{\mathbf{E}}^m_{Dn}(\mathbf{r}_{mn})\right)\frac{\exp(-ik_0 r_{mn})}{r_{mn}}\\ &= x_n\mathbf{E}_n(\theta,\,\varphi)\frac{\exp(-ik_0 r_{mn})}{r_{mn}},\end{aligned} \tag{5}$$

where $\mathbf{E}_n(\theta, \varphi)$ is the n-th element field (or far-field pattern) when the excitation current amplitude is unity. If the receiving far-field pattern of the probe $\mathbf{h}(\theta, \phi)$ is known, the antenna array diagnosis problem can be written in matrix form

$$\mathbf{U} = \mathbf{A}\mathbf{x} \tag{6}$$

https://doi.org/10.1017/S1759078719000989 Published online by Cambridge University Press

where $\mathbf{x} = (x_1, x_2, \ldots, x_N)^T \in C^N$ is an excitation vector, $\mathbf{U} = (U_1, U_2, \ldots, U_M)^T \in C^M$ is the measurement vector, i.e. complex amplitudes of voltage registered by the probe, and elements of the measurement matrix $\mathbf{A} \in C^{M\times N}$ can be found as

$$a_{mn} = \frac{U_m}{x_n} = \mathbf{E}_n(\theta_{mn}, \varphi_{mn}) \cdot \mathbf{h}(\theta'_{mn}, \varphi'_{mn}) \exp(-ik_0 r_{mn})/r_{mn} \quad (7)$$

The definition of angles θ, φ, θ', and φ' is shown in Fig. 2.

This formulation is correct for any array geometry and measurement surface S_M. It is also applicable to similar problems that can be reduced to the reconstruction of electric and/or magnetic currents, in the frequency domain or time domain [18]. Conventional methods require $M \geq N$ to solve (6), i.e. a full set of measurements is required. Due to several reasons, the measurement matrix $\mathbf{A}$ is ill-conditioned, so the convergence and accuracy of the solution degrade when the dimensionality of the problem grows [6].

Solution of CS problem

It is assumed that the excitation vector is sparse, i.e. the number of non-zero components K is significantly lower than total number of its elements N. For an array that has low number of defect elements, a vector that is a difference between defect array (AUT) and reference array (non-defect) can be found $\mathbf{x} = \mathbf{x}_r - \mathbf{x}_d$. Then (6) can be rewritten as

$$\mathbf{U}_d - \mathbf{U}_r = \mathbf{A}(\mathbf{x}_d - \mathbf{x}_r) \quad (8)$$

$$\mathbf{U} = \mathbf{U}_d - \mathbf{U}_r, \quad \mathbf{x} = \mathbf{x}_d - \mathbf{x}_r \quad (9)$$

Excitation vector $\mathbf{x}$ in (9) (see Fig. 3) corresponds to a "sparse" array that consists of a small number of radiating elements.

Note that the reference array excitation vector can be found by using the conventional diagnosis methods or by means of numerical modeling. If the number of measurements M is smaller than the number of elements N (the goal of using CS-based methods), the problem (8) is ill-posed and a regularization procedure is required. Usually some kind of *a priori* information about the solution is used, e.g. the sparseness of $\mathbf{x}$ for the CS-based methods. There are different ways to exploit the sparseness of $\mathbf{x}$ [9], for example, using the ℓ_0 norm:

$$\min\|\mathbf{x}\|_0: \quad \|\mathbf{Ax} - \mathbf{U}\|_2 < \varepsilon, \quad (10)$$

or using a more convenient $\ell_1$norm, which leads to a convex minimization problem:

$$\min\|\mathbf{x}\|_1: \quad \|\mathbf{Ax} - \mathbf{U}\|_2 < \varepsilon, \quad (11)$$

where $\|\ldots\|_2$ is Euclidean norm, $\|\mathbf{x}\|_1 = \sum_{n=1}^{N} |x_n|$ is $\ell_1$norm, ε is related to the noise affecting the data. The constrained minimization problem (11) can be rewritten as a ℓ_1/ℓ_2 minimization problem

$$\min_{\mathbf{x}} \|\mathbf{Ax} - \mathbf{y}\|_2^2 + \mu\|\mathbf{x}\|_1, \quad (12)$$

which can be efficiently solved using different iterative algorithms, e.g. YALL 1 [19] or NESTA [20,21].

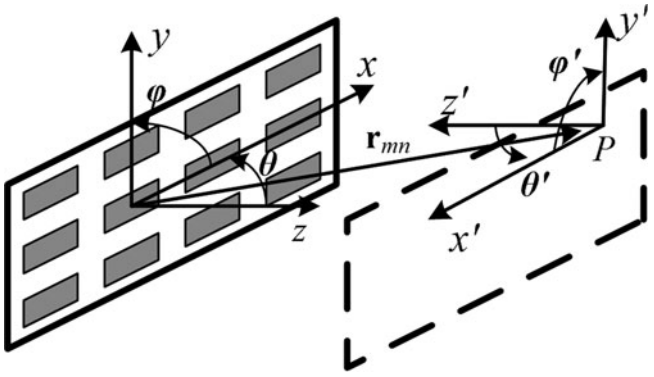


Fig. 2. Geometry of coordinate systems used for *n*-th radiating element and *m*-th position of the probe located at the point *P*.

The reliability and precision of solution depend not only on the signal-to-noise ratio (SNR), but also on the measurement matrix, i.e. the positions of measurement points. If a measurement matrix satisfies the so-called restricted isometry property (RIP) [9,10], then the excitation vector can be reliably reconstructed with high precision. Calculation of RIP requires proof for all K-sparse $\mathbf{x}$ vectors, which is usually impractical. For far-field array diagnosis, an approach to the deterministic selection of measurement points is presented in [13]. In a near-field diagnosis case discussed in [14], a 368-element circular array is effectively diagnosed using 24 measurement points, whose positions were determined by numerical trials.

Even if the optimal positions of the probe are found, there still are other issues that need to be solved before CS-based methods could be used in practice. They are described in the next section.

Known issues of the method and proposed solutions

The CS-based diagnosis has a high probability of detection of defect elements and allows reconstructing amplitude and phase of the elements with high precision when the two conditions are met. First, the measurement matrix $\mathbf{A}$ must be known with high precision; second, it is assumed that the excitations of non-defect elements in reference and defect arrays are exactly the same. Both assumptions are rarely true. Far-field patterns of the probe and array elements in equation (7) are not always known exactly, and equation (7) is true only for anechoic conditions. The difference in the excitation of non-defect elements is caused by the mutual coupling of the radiators and by the thermal instability of active elements.

While the performance of CS-based diagnosis method deteriorates in the presence of errors mentioned above, this method can still locate defective elements, albeit with lower precision and reliability [5]. To improve precision and probability of detection, we propose two modifications of this method, which can be used independently or jointly.

Low reconstruction accuracy

First modification of the method addresses an issue with exact values of measurement matrix $\mathbf{A}$. The only practically feasible way of obtaining $\mathbf{A}$ with high precision implies direct measurements of the field of every single element at every

https://doi.org/10.1017/S1759078719000989 Published online by Cambridge University Press

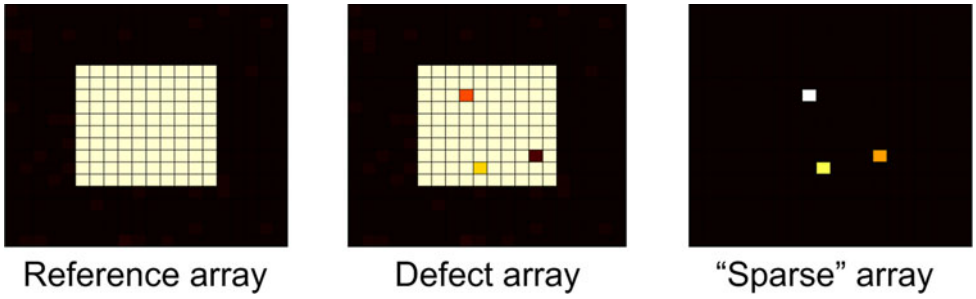


Fig. 3. An illustration of 10 × 10 "sparse" array construction.

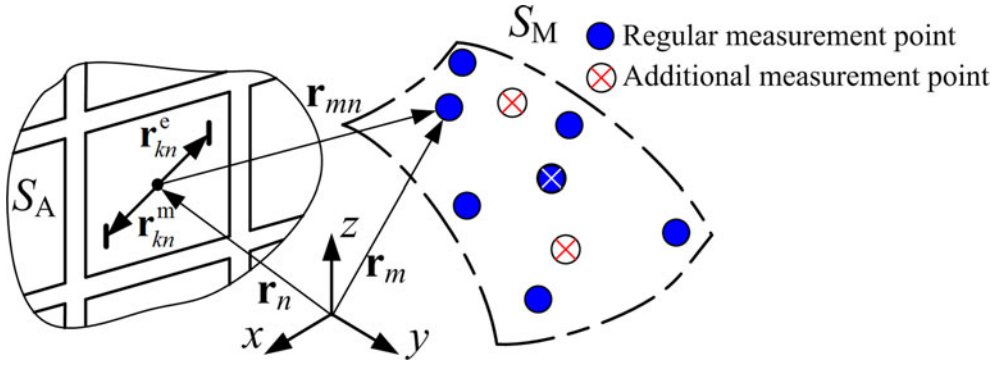


Fig. 4. Geometry of acquisition for additional measurements.

measurement point (7). This process is very time-consuming and requires AUT to be placed exactly in the same position as a reference array. This leads us to the two-step algorithm. In the first step, the radiating elements are separated into two groups: normally operating elements and potentially defect elements using CS-based diagnosis. The second step is required to separate the defect elements and operating elements from the set of potentially defect elements. To do so, the additional measurement set is conducted at a selected measurement point m (or a set of selected additional measurement points, see Fig. 4), for which a_{mn}, $n = 1,\ldots, N$, is known with required high accuracy.

For each potentially defect element, the excitation phase is increased (using phase shifters of AUT) by the specified value $\Delta\varphi$, e.g. 180°, leaving the excitations of other elements unchanged. For k-th defect element, the complex amplitudes of the measured field at the measurement point can be found as

$$\dot{U}^k_{\Sigma 1} = \dot{U}^k_{\Sigma 0} + \dot{U}^k = \sum_{n=1,\ n\neq k}^{N} \left(\dot{U}^d_n - \dot{U}^r_n\right) + \dot{U}^d_k - \dot{U}^r_k$$

$$\dot{U}^k_{\Sigma 2} = \dot{U}^k_{\Sigma 0} + \dot{U}'^k = \sum_{n=1,\ n\neq k}^{N} \left(\dot{U}^d_n - \dot{U}^r_n\right) + \dot{U}^d_k \times \exp(i\Delta\varphi) - \dot{U}^r_k, \tag{13}$$

where $\dot{U}^k_{\Sigma 1}$, $\dot{U}^k_{\Sigma 0}$, and $\dot{U}^k$ are the complex amplitudes (before changing the phase of k-th element) of the measured field, field of all elements except k-th element and field of k-th element only, respectively. $\dot{U}^k_{\Sigma 2}$ and $\dot{U}'^k$ are the complex amplitudes (after changing the phase) of the measured field and of k-th element field, respectively. Transforming (13), the field produced by k-th defect element can be found as

$$\dot{U}^d_k = \frac{\dot{U}^k_{\Sigma 1} - \dot{U}^k_{\Sigma 2}}{1 - \exp(i\Delta\varphi)} \tag{14}$$

Note that $\dot{U}^k_{\Sigma 1} - \dot{U}^k_{\Sigma 2}$ may be zero in case the amplitude of k-th element is zero, or in case of phase shifter failure when $\Delta\varphi = 0$. The element will be classified as a defect in both cases.

The complex amplitude of k-th element excitation can be found from (6) as

$$\dot{x}^d_k = \frac{\dot{U}^d_k}{\dot{a}_{mk}} \tag{15}$$

or, if using expression (7):

$$\dot{x}^d_k = \frac{\dot{U}^d_k r_{mk} \exp(ik_0 r_{mk})}{h(\theta'_{mk}, \varphi'_{mk}) E(\theta_{mk}, \varphi_{mk})} \tag{16}$$

Thermal instability of the array

Second modification of the method addresses the issue of thermal instability of the array. Changes in excitation are usually modeled in the same way as thermal noise (e.g. [14]), but thermal instability error has a non-zero mean value because changes in temperature lead to approximately the same change of amplitude and phase of all elements. It means that vector $\mathbf{x} = \mathbf{x}_d - \mathbf{x}_r$ is no longer sparse and non-defect elements could be categorized as a defect.

https://doi.org/10.1017/S1759078719000989 Published online by Cambridge University Press

Table 1. Excitations of defect elements

	1	2	3	4	5	6	7	8	9	10
Amplitude	0.707	1.0	0.9	0.5	0.9	0.707	1.0	0.3	0.8	1.2
Phase	90°	−45°	90°	0	−30°	0°	30°	−20°	60°	−25°

To solve this problem we assume that all elements change their amplitudes and phases equally. This assumption is true when temperature changes only slightly (several °C) and there is no significant variation in temperature across the array. In practice, it means that the reference and defect arrays are the same, e.g. when the reference array is measured, then tested (mechanically/thermally) and then is measured again at the same thermal conditions as before to check whether any active elements have failed.

In this case, the measured field of AUT $\mathbf{U}_d^m$ can be found as

$$\mathbf{U}_d^m = p_c \mathbf{U}_d, \quad p_c = a_c \exp(i\varphi_c), \tag{17}$$

where p_c is a correction coefficient and $\mathbf{U}_d$ is the field that would be measured in the absence of thermal instability. Then equation (9) takes the form

$$\mathbf{U} = \frac{\mathbf{U}_d}{p_c} - \mathbf{U}_r, \ \mathbf{x} = \frac{\mathbf{x}_d}{p_c} - \mathbf{x}_r \tag{18}$$

To determine the correction coefficient p_c the minimization problem (12) should be solved for different values of p_c.

$$\min_{p_c} \left\| \mathbf{A}\mathbf{x}_f - (\mathbf{U}_d^m p_c^{-1} - \mathbf{U}_r) \right\|_2^2 + \mu \left\| \mathbf{x}_f \right\|_1, \tag{19}$$

where $\mathbf{x}_f$ is a solution of (12) for a given value of p_c. Function minimized in (19) is convex, in the absence of noise its minimum corresponds exactly to correction coefficient p_c.

It should be noted that all CS methods are based on *a priori* information about the solution (the assumption that the solution is sparse). Hence the proposed procedure is only useful when (17) is at least approximately true. If thermal changes also affect the phase-distribution network, or if AUT is so large that the temperature is different across the array, then the algorithm cannot improve the solution. In this case, more precise *a priori* information or more measurements are required to reconstruct the excitation successfully.

Results and discussion

To determine the validity of our approach, we conducted a numerical experiment. We want to find answers to the following questions:

- How important is the accuracy of the measurement matrix and how does it affect the solution?
- How can we improve the accuracy using the approach proposed in section "Low reconstruction accuracy"? How does the thermal instability affect the reconstruction results and how can we improve it using the procedure described in section "Thermal instability of the array"?

The parameters of the experiment are provided in the next subsection.

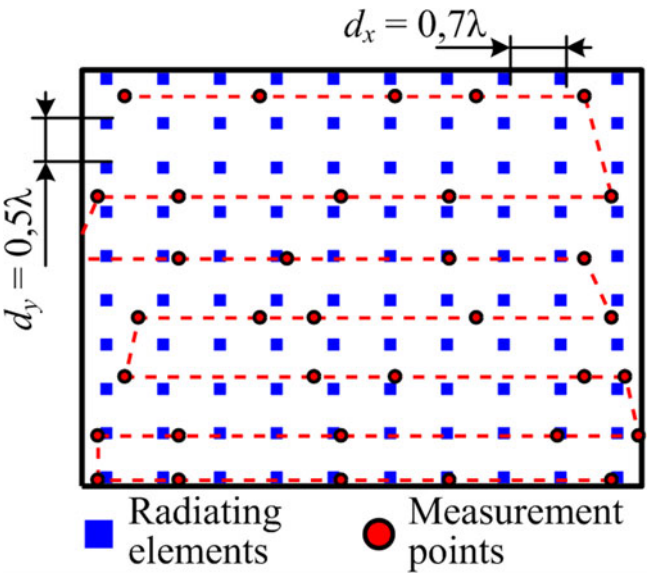


Fig. 5. Positions of radiating elements and measurement points.

Model of the array and experiment parameters

A planar rectangular 10×10 array of open waveguide elements is considered, the field of the array was simulated with FDTD. While CS-based diagnosis methods do not strictly require the measurement surface to be planar, it is common to measure the field of a planar array on a plane parallel to the aperture [7]. To ensure that the measurement points are in the far-field region of any radiating element (but not in the far-field of the array itself), we have chosen the distance between the measurement plane and the aperture of the array to be equal 3λ, where λ is the operating wavelength. To show the ability of CS-based methods to solve the underdetermined problem (9), we have chosen the number of measurements lower than the number of elements, in our case $M = 35$. It is possible that this number could be improved if another measurement geometry was used, but, as noted in the Introduction, the problem of optimal measurement point selection in the near-field case has not been solved yet.

The effectiveness of a diagnosis method may be characterized in many different ways, but in our case, two values are of particular interest: failure identification success rate (FISR) and PFD. FISR is the probability of locating all defect elements, and PFD is the average number of false detections per a non-defect element of the array:

$$\text{PFD} = \frac{\text{Average } N \text{ of false detections in solution}}{N \text{ of non-defect elements}} \tag{20}$$

The accuracy and precision of the method were also investigated. Since l_1-based reconstruction methods are known to underestimate high-amplitude components [22,23], we have computed both the mean value of the error and its standard deviation (SD).

https://doi.org/10.1017/S1759078719000989 Published online by Cambridge University Press

Table 2. Parameters of the model

Number of elements	Number of defects	Distance to measurement plane	Number of measurements	Amplitude accuracy	Phase accuracy
100	3…10	3λ	35	±5%	±2°

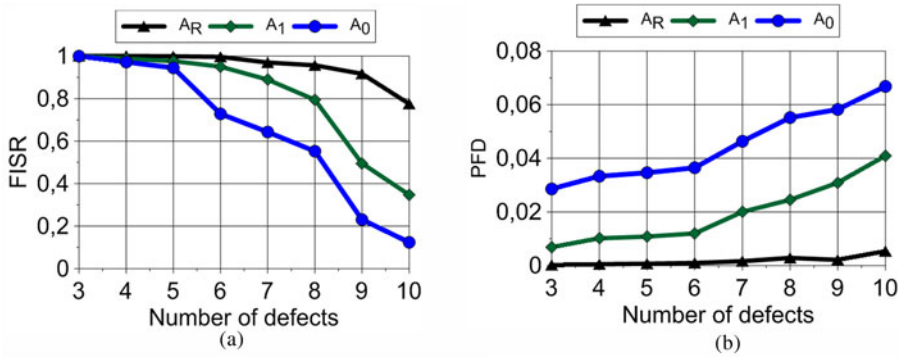


Fig. 6. Characteristics of the diagnosis method for a 10 × 10 array of open waveguide elements with 3λ distance to measurement plane: (a) failure identification success rate (FISR) and (b) probability of false detections (PFD). $\mathbf{A}_R$ – results acquired using the reference measurement matrix, $\mathbf{A}_0$ – "simplified" measurement matrix, $\mathbf{A}_1$ – "approximate" measurement matrix.

The excitation of the reference array was uniform. In a defect array, 3–10 (to keep the number of defects K much lower than the number of elements N) defect elements with excitations specified in Table 1 were present. All non-defect elements have an amplitude of 1 and phase 0°.

The radiation pattern $\mathbf{E}_n$ of n-th radiating element in equation (7) is not always known exactly, and elements of a calculated measurement matrix may differ from the measured ones. In order to determine how errors in the measurement matrix influence the solution, diagnosis problem (12) was solved using three different measurement matrices. The "exact" (or "reference") measurement matrix $\mathbf{A}_R$ is acquired by simulating sequential excitation of every single element. For the "simplified" measurement matrix $\mathbf{A}_0$ all elements were assumed isotropic ($\mathbf{E}_n = 1$ for all n). The "approximate" measurement matrix $\mathbf{A}_1$ was calculated using a quasi-analytical far-field pattern of an open waveguide $\mathbf{E}_n$.

Positions of the elements and measurement points are shown in Fig. 5.

The n-th element was considered a defect when the absolute value of x_n (n-th component of the vector $\mathbf{x} = \mathbf{x}_d - \mathbf{x}_r$) was larger than a certain threshold. In this paper, this threshold was set to 0,1, which corresponds roughly to ±1 dB amplitude error (to detect defects of discrete attenuators with a least significant bit of 0.5…1 dB) or ±6° phase error (to detect defects of 6-bit discrete phase shifters with a least significant bit of 5625°).

Finally, we assume that the accuracy of amplitude and phase measurement is about ±5% and ±2°, respectively. This accuracy roughly corresponds to an SNR of 40 dB stated in [24].

All parameters of the model are combined in Table 2.

Results of diagnosis without correction

For a given number of defects, FISR and PFD were estimated by repeating the identification procedure 2000 times (100 different distributions of defect elements, 20 different realizations of white Gaussian noise for each distribution). Results of diagnosis (FISR and PFD) in thermally stable conditions are shown in Figs 6(a) and 6(b).

As it could be expected from the results presented in [14], FISR decreases with the number of defect elements. For a small number of defects, FISR is high no matter what measurement matrix was used; the only real difference is PFD. For 10 defects, PFD obtained using $\mathbf{A}_R$ and $\mathbf{A}_0$ differ more than 10 times.

The accuracy of amplitude and phase reconstruction is shown in Fig. 7. It was expected that the results obtained using the simplest measurement matrix $\mathbf{A}_0$ will have the lowest precision (high SD), and the better we know the measurement matrix, the more accurate and precise results we get. It can also be seen that matrices $\mathbf{A}_R$ and $\mathbf{A}_1$ produce an accurate and precise value of the elements' phase.

However, if the matrices $\mathbf{A}_R$ and $\mathbf{A}_1$ cannot be obtained, we need a way to increase the accuracy and precision of excitation reconstruction. Our first modification of CS method addresses this issue, and the simulated results of its implementation are presented in the next subsection.

Accuracy improvement using additional measurements

After potentially defect elements were identified using the CS-based diagnosis method, we may need to improve the accuracy and precision of excitation reconstruction. To do so, we conduct additional measurements at a single point in the center of the measurement plane. The additional phase shift was equal to 180°.

Usually the duration of the near-field measurement is determined by the scanner movement, and not by the measurement of the field samples. Since the probe is fixed now, we can increase the duration of each measurement and thus increase the accuracy of amplitude and phase measurement without increasing overall measurement time too much. It may be required when we try to separate the signal of a single element from signals of all other elements. For our simulations, we assumed amplitude and phase accuracy of ±3% and ±1°, respectively.

https://doi.org/10.1017/S1759078719000989 Published online by Cambridge University Press

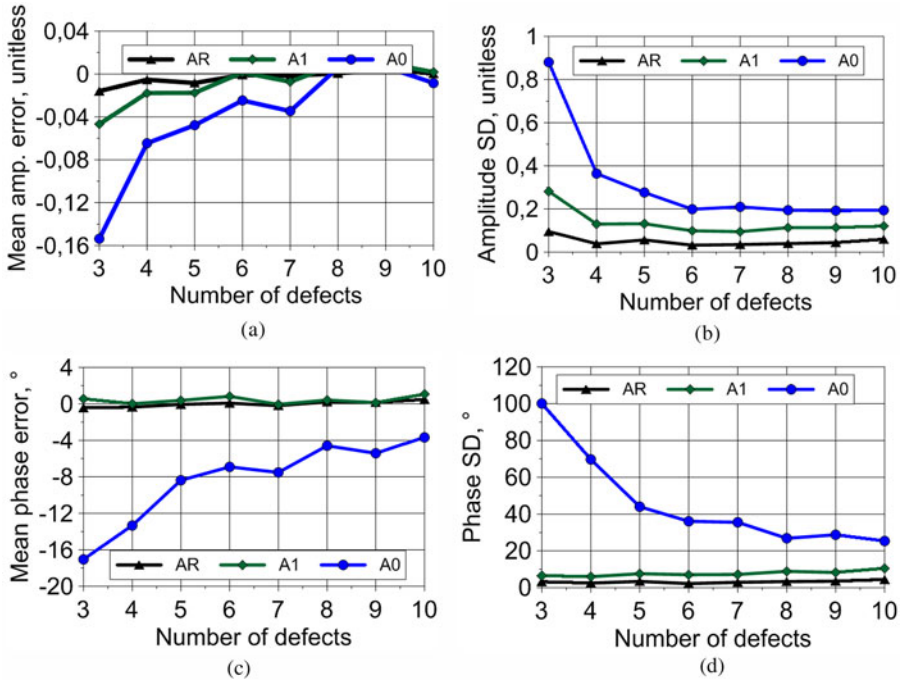


Fig. 7. Accuracy and precision of excitation reconstruction: (a) mean of amplitude error; (b) standard deviation (SD) of amplitude error, (c) mean of phase error; (d) SD of phase error.

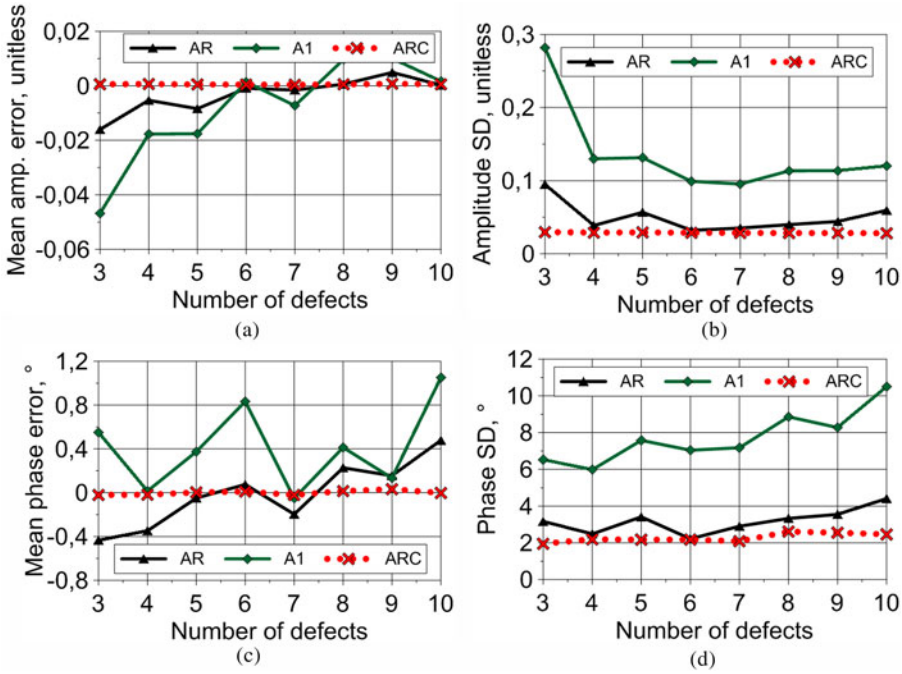


Fig. 8. Accuracy and precision of excitation reconstruction: (a) mean of amplitude error; (b) SD of amplitude error; (c) mean of phase error, (d) SD of phase error. $\mathbf{A}_R$ – reconstructed using reference measurement matrix, $\mathbf{A}_1$ – using approximate measurement matrix, ARC – corrected results.

The analysis of results shown in Fig. 8 confirms that the accuracy of the proposed has increased significantly. Mean value of error is zero; amplitude and phase are reconstructed with a precision of 0.1 and 6°, respectively. It should be noted again that a row of the measurement matrix a_{mn}, $n = 1 \ldots N$ for a given m should be known, i.e. measured. Mean value of phase error (see Fig. 8(c)) is close to the measurement accuracy (approximately 1°).

Correction of solution in the presence of thermal instability effects

Now we try to determine how thermal instability affects the solution. In our case, a change in temperature of the array leads to the change in the excitation of all array elements. We assume that the change in temperature is equal for all elements, and that their amplitudes and phases change by the same amount. In this simulation, a 0.42 dB

https://doi.org/10.1017/S1759078719000989 Published online by Cambridge University Press

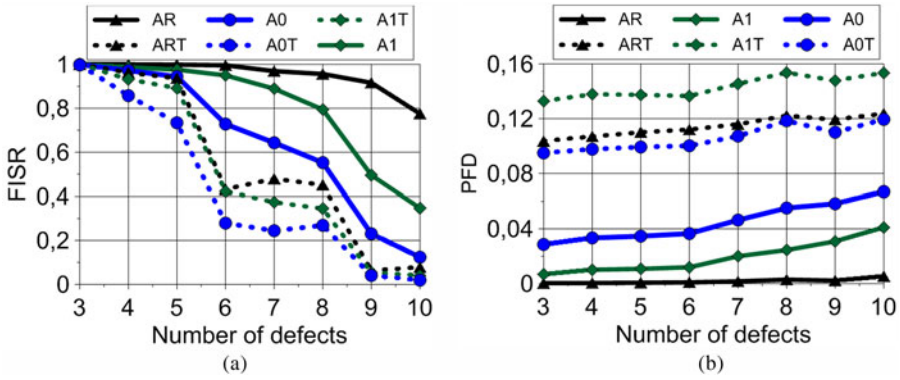


Fig. 9. (a) FISR and (b) PFD in the presence of thermal instability compared to initial results. $\mathbf{A}_R$, $\mathbf{A}_0$, $\mathbf{A}_1$ – initial results (in the absence of thermal changes, see Fig. 6), $\mathbf{A}_R T$, $\mathbf{A}_0 T$, $\mathbf{A}_1 T$ – results in the presence of thermal instability.

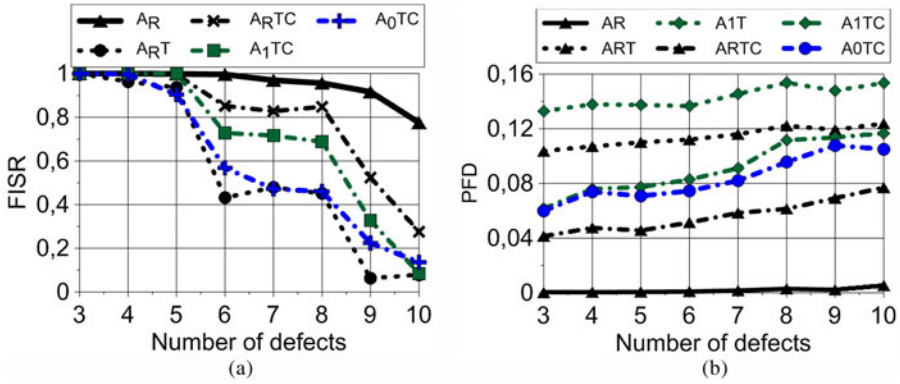


Fig. 10. Results of diagnosis correction procedure (19): (a) FISR and (b) PFD.

change in amplitude and 1° change in the phase were assumed. The FISR and PFD obtained under these conditions are shown in Fig. 9.

It can be seen from the results presented in Fig. 9 that the thermal instability of the array significantly reduces the effectiveness of the CS-based diagnosis. As expected, the number of false detection increases (2–20 times compared to initial PFD). It should be noted that for a small number of elements (<5% of all elements) the probability of detection remains sufficiently high (90% and higher) for results acquired with measurement matrices $\mathbf{A}_R$ and $\mathbf{A}_1$. Unfortunately, FISR rapidly decreases with a larger number of defects.

The results (FISR and PFD) of correction procedure (19) applied to the same 10×10 array are presented in Fig. 10.

As can be seen from Fig. 10, the correction procedure can significantly increase the identification success rate and reduce PFD. For example, for 6–8 defects, FISR improved from approximately 50 to 85% using a reference measurement matrix $\mathbf{A}_R$. However, when the measurement matrix is not known exactly, the performance of this diagnosis method degrades again. While five defect elements or less can be recovered with high probability (>90% for any measurement matrix), increasing number of defects to six or more leads to a much lower detection probability.

Conclusion

In this paper, we have investigated a CS-based antenna array diagnosis method and presented two modifications. These modifications deal with the two disadvantages of the method: sensitivity to thermal instability of active elements of the array (or to any other source of error with non-zero mean value) and low accuracy of excitation reconstruction.

Our research has shown that the thermal instability greatly reduces the usefulness of the CS-based diagnosis method, increasing the number of false detections up to 20 times. It also lowers the number of defect elements that can be reconstructed with a required probability of success.

The first proposed modification is based on a modified l_1-minimization procedure and allows correcting the measured field in case of thermal instability of the array. For example, FISR was reduced from 95 to 40% (six defects in a 100-element array), but the correction procedure increased it to 85%.

The second proposed modification increases the accuracy of excitation reconstruction by using several additional measurements. It requires the data about the exact (directly measured) row of a measurement matrix and the ability to change the phase of a single radiating element. Contrary to the CS-based only reconstruction, the resulting accuracy of reconstruction depends only on field measurement accuracy at the measurement point.

Acknowledgement. This work was supported by the Ministry of Education and Science of the Russian Federation under the agreement of 14.577.21.0279 of 26.09.2017, ID RFMEFI57717X0279.

References

1. **Bachmann M, Schwerdt M and Brautigam B** (2009) Accurate antenna pattern modeling for phased array antennas in SAR applications –

https://doi.org/10.1017/S1759078719000989 Published online by Cambridge University Press

demonstration on TerraSAR-X. *International Journal of Antennas and Propagation* **2009**, Article ID 492505.
2. **Stangl M, Werninghaus R, Schweizer B, Fischer C, Brandfass M, Mittermayer J and Breit H** (2006) TerraSAR-X technologies and first results. *IEE Proceedings – Radar, Sonar and Navigation* **2**, 86–95.
3. **Brautigam B, Schwerdt M and Bachmann M** (2009) An efficient method for performance monitoring of active phased array antennas. *IEEE Transactions on Geoscience and Remote Sensing* **4**, 1236–1243.
4. **Sanchez V, Martin F, Barrio A, Pinto I, Garcia R, Sierra M, De Haro L, Besada JL and Galocha B** (2017) Measurement of BepiColombo mission medium gain antenna parameters under realistic thermal conditions. *International Journal of Microwave and Wireless Technologies* **9**, 1409–1418.
5. **Kuznetsov GY, Miloserdov MS, Temchenko VS, Kovalenko AI, Voskresenski DI, Vnotchenko SL, Riman VV and Shishanov AV** (2017) Practical aspects of active phased arrays characterization during thermal testing. *Progress in Electromagnetics Research Symposium – Spring (PIERS), St. Petersburg, Russia.*
6. **Bucci OM, Migliore MD and Panariello G** (2005) Accurate diagnosis of conformal arrays from near-field data using the matrix method. *IEEE Transactions on Antennas and Propagation* **3**, 1114–1120.
7. **Wang JJH** (1988) An examination of theory and practices of planar near-field measurement. *IEEE Transactions on Antennas and Propagation* **6**, 746–753.
8. **Alvarez Y, Las-Heras F and Garcia C** (2012) The sources reconstruction method for antenna diagnostics and imaging applications. *Solutions and Applications of Scattering, Propagation, Radiation and Emission of Electromagnetic Waves, IntechOpen, London*, pp. 159–186.
9. **Migliore MD** (2011) A compressed sensing approach for array diagnosis from a small set of near-field measurements. *IEEE Transactions on Antennas and Propagation* **6**, 2127–2133.
10. **Rauhut H** (2009) Compressive sensing and structured random matrices. *Radon Series on Computational and Applied Mathematics* **9**, 1–94.
11. **Shah P and Khankhoje UK and Moghaddam M** (2016) Inverse scattering using a joint L1-L2 norm-based regularization. *IEEE Transactions on Antennas and Propagation* **4**, 1373–1384.
12. **Turk AS, Ozkan-Bakbak P, Durak-Ata L, Orhan M and Unal M** (2016) High-resolution signal processing techniques for through-the-wall imaging radar systems. *International Journal of Microwave and Wireless Technologies* **8**, 855–863.
13. **Li W, Deng W and Migliore MD** (2018) A deterministic far-field sampling strategy for array diagnosis using sparse recovery. *IEEE Antennas and Wireless Propagation Letters* **7**, 1261–1265.
14. **Pinchera D and Migliore MD** (2017) Failure identification and pattern correction in large isophoric sparse arrays. *European Conference on Antennas and Propagation (EUCAP), Paris, France*.
15. **Kuznetsov GY, Miloserdov MS, Bulygin ML, Temchenko VS, Kovalenko AI and Riman VV** (2018) Near-field measurement techniques for space-borne SAR digital phased array antennas. *12 European Conference on Synthetic Aperture Radar (EUSAR 2018), Aachen, Germany.*
16. **Kuznetsov GY, Temchenko VS, Miloserdov MS and Voskresenskiy DI** (2018) Phased antenna array reconstructive diagnostics using small number of measurements. *2018 Baltic URSI Symposium, Poznan, Poland.*
17. **Hansen TB** (2009) Complex-point dipole formulation of probe-corrected cylindrical and spherical near-field scanning of electromagnetic fields. *IEEE Transactions on Antennas and Propagation* **3**, 728–741.
18. **Kuznetsov Y, Baev A, Gorbunova A, Konovalyuk M, Thomas D, Smartt C, Baharuddin MH, Russer JA and Russer P** (2016) Localization of the equivalent sources on the PCB surface by using ultra-wideband time domain near-field measurements. *2016 International Symposium on Electromagnetic Compatibility – EMC Europe, Wroclaw, Poland.*
19. **Yang J and Zhang Y** (2011) Alternating direction algorithms for l_1-problems in compressive sensing. *Society for Industrial and Applied Mathematics* **1**, 250–278.
20. **Becker S, Bobin J and Candes EJ** (2011) NESTA: a fast and accurate first-order method for sparse recovery. *SIAM Journal on Imaging Sciences* **4**, 1–39.
21. **Nesterov Y** (2005) Smooth minimization of non-smooth functions. *Mathematical Programming* **5**, 127–152.
22. **Selesnick I** (2017) Sparse regularization via convex analysis. *IEEE Transactions on Signal Processing* **9**, 4481–4494.
23. **Wei Z, Zhang B, Han B, Xu Z, Hong W and Wu Y** (2018) An accurate SAR imaging method based on generalized minimax concave penalty. *12 European Conference on Synthetic Aperture Radar (EUSAR 2018), Aachen, Germany.*
24. IEEE recommended practice for near-field antenna measurements (2012). https://doi.org/10.1109/IEEESTD.2012.6375745



Grigory Kuznetsov received his Ph.D. in engineering from the Moscow Aviation Institute in 2018. He is now a researcher at the Research Institute of Precision Instruments. His main research interests are antenna design and measurement, as well as synthetic aperture radar systems.



Vladimir Temchenko received his Ph.D. in 1982 and Dr Sc (Eng) in 2012 from the Moscow Aviation Institute. He is currently a professor of "Radiophysics, antennas, and microwave devices" chair at the Moscow Aviation Institute and his main research interests include antenna measurement and diagnosis, inverse scattering problems as well as ground-penetrating radar.



Maxim Miloserdov received his Ph.D. in 2014 from the Department of Radioelectronics of the Moscow Aviation Institute. He is now a researcher at the Research Institute of Precision Instruments. His current research interests include active phased arrays, their characterization, and applications in synthetic aperture radar.



Dmitry Voskresenskiy received his Diploma and Ph.D. at the Moscow Aviation Institute in 1951 and 1955, respectively. He received a Dr Sc (Eng) in 1966 from the Moscow Aviation Institute. He is a chair of the antenna chair of the Department of Radioelectronics at the Moscow Aviation Institute since 1975. He has authored more than 200 research articles and his current research interests include phased antenna arrays and their components.

https://doi.org/10.1017/S1759078719000989 Published online by Cambridge University Press